Int. J. Electrochem. Sci., 6 **(2011)** 6184 - 6199

International Journal of ELECTROCHEMICAL SCIENCE
www.electrochemsci.org

Corrosion Passivation in Simulated Body Fluid of Magnesium/Hydroxyapatite Nanocomposites Sintered by High Frequency Induction Heating

Khalil Abdelrazek Khalil [1, 3, *], *El-Sayed M. Sherif* [2, 4] *and Abdulhakim A. Almajid* [1, 2]

[1] Mechanical Engineering Department, (CEREM), College of Engineering, King Saud University P.O. Box 800, Riyadh 11421
[2] Center of Excellence for Research in Engineering Materials (CEREM), College of Engineering, King Saud University, P.O. Box 800, Riyadh 11421, Saudi Arabia
[3] Material Engineering and Mechanical Design Department, Faculty of Energy Engineering, South Valley University, Aswan, Egypt
[4] Electrochemistry and Corrosion Laboratory, Department of Physical Chemistry, National Research Centre (NRC), Dokki, 12622 Cairo, Egypt
[*]E-mail: kabdelmawgoud@KSU.EDU.SA

Received: 29 September 2011 / *Accepted:* 5 November 2011 / *Published:* 1 December 2011

Super fast densification behavior and the attendant corrosion features of magnesium/hydroxyapatite (Mg/HAp) bio-nanocomposites processed by high frequency induction heat sintering (HFIHS) were investigated in order to develop a new biodegradable hard tissue substituent. Mg/HAp nanocomposite with various HAp contents (0-5 wt %) were prepared using pure magnesium and HAp nanopowder as raw materials. In order to investigate the corrosion behavior of Mg/HAp in vitro, the composite samples were immersed in a simulated body fluid (SBF) at 37℃. The electrochemical tests were conducted under the same condition. The results indicated that the presence of HAp and the increase of its content decreased the dissolution of Mg and improve the resistance of magnesium against uniform corrosion, while increase the probability of the occurrence of localized corrosion. The best performance against corrosion in SBF solution was obtained for Mg/5.0wt%HAp. The EIS experiments were carried out to determine kinetic parameters for electron transfer reactions at the electrode/electrolyte interface magnesium in SBF solution. The values of resistances, R_S, R_{P1}, R_{P2} and R_{P3} increased in the presence of HAp and the increase of its content from 1wt% to 5 wt%. This effect also decreased the values of the C_{dl1}, *CPE*, and C_{dl2} and indicates that HAp particles improve the corrosion resistance of magnesium in SBF solution and its effect increases with increasing HAp concentration. The impedance of the interface (|Z|) of Mg increased in the presence and by the increase of HAp. In this work, the Mg/1 to 3 wt% HAp composite was of the optimal mechanical properties and corrosion resistance.

Keywords: hydroxyapatite; magnesium alloys; nanocomposites; corrosion passivation; high frequency induction heat sintering

1. INTRODUCTION

Magnesium alloys are currently used in many structural applications. It is believed that magnesium and its alloys may also find applications in biomedical fields. Devices for use within the body must be able to withstand corrosion in a biological environment and endure use for years without undue wear (and without causing damage to surrounding tissues). Before insertion, they should be unchanged during storage, and must be sterilized without damage. The thermal and chemical stability of biomaterials, high strength, wear resistance and durability all contribute to making composites good candidate materials for surgical implants. Recently, magnesium alloys have attracted much attention as potential biodegradable bone implant materials due to their biodegradability in the bioenvironment [1–3], and their excellent mechanical properties such as high strength and possessing an elastic modulus close to that of bone [4]. However, the rapid corrosion of magnesium alloys in chloride containing solutions including human body fluid or blood plasma has limited their clinical applications [4, 5]. Therefore, it is very important to improve the corrosion resistance of magnesium alloys in order for them to be applied clinically. Element alloying has been studied for developing biodegradable magnesium alloys with good mechanical and corrosion properties. Mn and Zn were selected as the alloying elements to develop Mg–Mn–Zn alloys due to the good biocompatibility of Mn and Zn [6, 7]. The addition of Mn and Zn improves both the mechanical properties and the corrosion resistance of magnesium alloys. It has been shown that the corrosion resistance of an Mg–1.0 Mn–1.0 Zn alloy in simulated body fluid (SBF) is slightly better than that of the WE43 alloy (containing 3.78 wt.% Y, 2.13 wt.% Nd and 0.46 wt.% Zr), which is one of the best commercially available magnesium alloys [8]. Furthermore, materials for surgical implants and medical devices must, before all else, be non-toxic. Ceramics, though they include good chemical and corrosion-resistant properties, are notoriously brittle. Researchers therefore have sought ways of combining desirable ceramics with other materials to tailor properties such as strength and elasticity to meet system requirements. Composites, functionally gradient materials, and coatings have been studied to optimize material choices. The bioceramic material most often used for bone replacement is hydroxyapatite or HAp [Ca_{10} $(PO_4)_6$ $(OH)_2$]. HAp has proven a very attractive material for bone replacement due to its close resemblance to vertebrate bone mineral and good bioactivity [9-12]. Much work has been devoted to the interfacial reactions of biological systems with hydroxyapatite, a ceramic with chemical structure very similar to the hard structure of bone. Hydroxyapatite is used as a coating for metal surgical implants (most often made of titanium and its alloys, or stainless steels), and recent studies have examined the possibility of its use in composite form, in materials that combine polymers with ceramic or metal/ceramic combinations. Considerable research has been performed on methods of coating application and in-situ synthesis of appetites, and the implications for ceramic properties and microstructure.

On the other hand, the technique of HFIHS has been shown to be an effective sintering method which can successfully consolidate ceramics and metallic powders to near theoretical density [13-15]. Wrap a coil of wire around chunk of metal or ceramic and feed the coil with high frequency, high power A.C. current, and before long time, the metal will be red hot and then molten. This is the main idea of using high frequency induction heating as a novel method for sintering metals and ceramics. It is similar to hot pressing, which is carried out in a graphite die, but the heating is accomplished by a

source of high frequency electricity to drive a large alternating current through a coil. This coil is known as the work coil. The passage of current through this coil generates a very intense and rapidly changing magnetic field in the space within the work coil. The workpiece to be heated is placed within this intense alternating magnetic field. The alternating magnetic field induces a current flow in the conductive workpiece.

In this study, super fast densification behavior and the attendant corrosion features of magnesium/hydroxyapatite bio-nanocomposites processed by high frequency induction heat sintering (HFIHS) were investigated. The aim is also extended to study the effect of different percentages of hydroxyapatite, namely 1, 2, 3 and 5 %, on the corrosion behavior of pure magnesium after their immersion in simulated body fluid (SBF). To achieve this objective, the study was carried out using different electrochemical techniques such as cyclic potentiodynamic polarization, chronoamperometric current-time variations, and electrochemical impedance spectroscopy.

2. EXPERIMENTAL PROCEDURE

In this study, Magnesium powder of 98.5% purity with a size range of 30–100 nm obtained from Merck KGaA, Germany, was used as the matrix material. Hydroxyapatite (HA) nanopowder of 99.0% purity with a size of around 50 nm obtained from Sigma Aldrich Corporation, USA, was used as the reinforcement. The starting grain size has been established by inspection of grain mounts using a Field Emission Scanning Electron Microscope (FE-SEM). The FE-SEM micrographs of the used powders are shown in Fig. 1. The powder has been checked for purity by X-ray diffraction as plotted in Fig. 2.

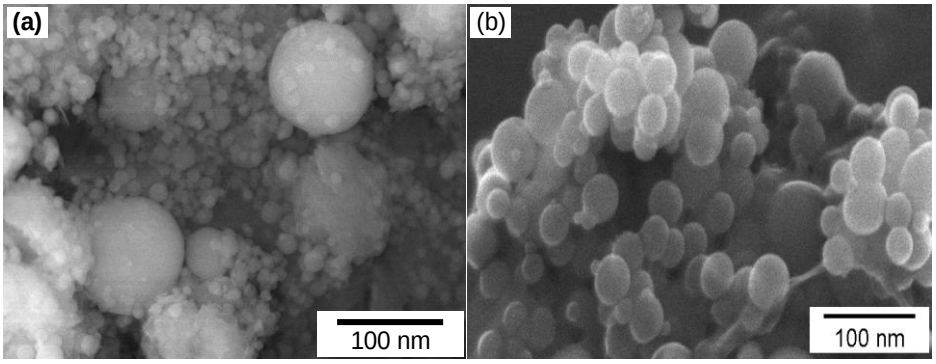

Figure 1. SEM micrographs of (a) magnesium and (b) hydroxyapatite powders

The measured crystal size for magnesium and hydroxyapatite were 51 and 41 nm respectively, as was measured by Scherrer formula. Experiments have been conducted on the processing of nanostructured magnesium 1-5wt% hydroxyapatite nanocomposites. Pure magnesium and hydroxyapatite nanopowder were weighed carefully in an argon-filled glovebox. All powders were milled in FRITCSH-Germany, mechanical alloying machine using zirconia balls and a rotation speed

of 200 rpm for 30 min with a ball-to-powder weight ratio of 5:1. The milling conditions were the same for all the powders. The blended powders were placed in the graphite die and then introduced into the high-frequency induction heat sintering (HFIHS). The basic configuration of a HFIHS unit is shown in Figure 3.

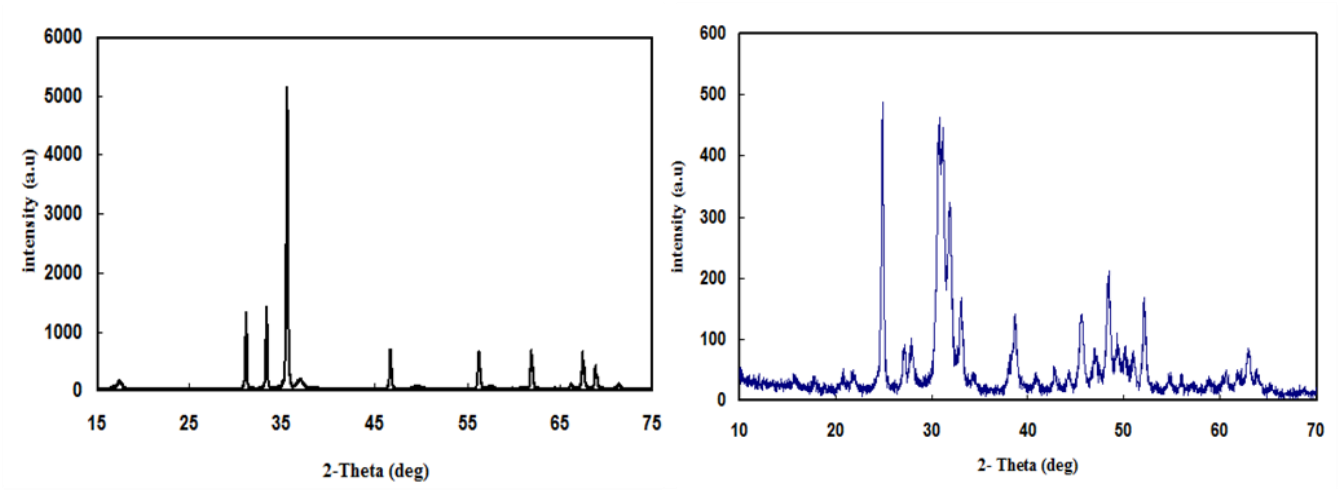

Figure 2. XRD pattern of the as received magnesium and hydroxyapatite powders, respectively.

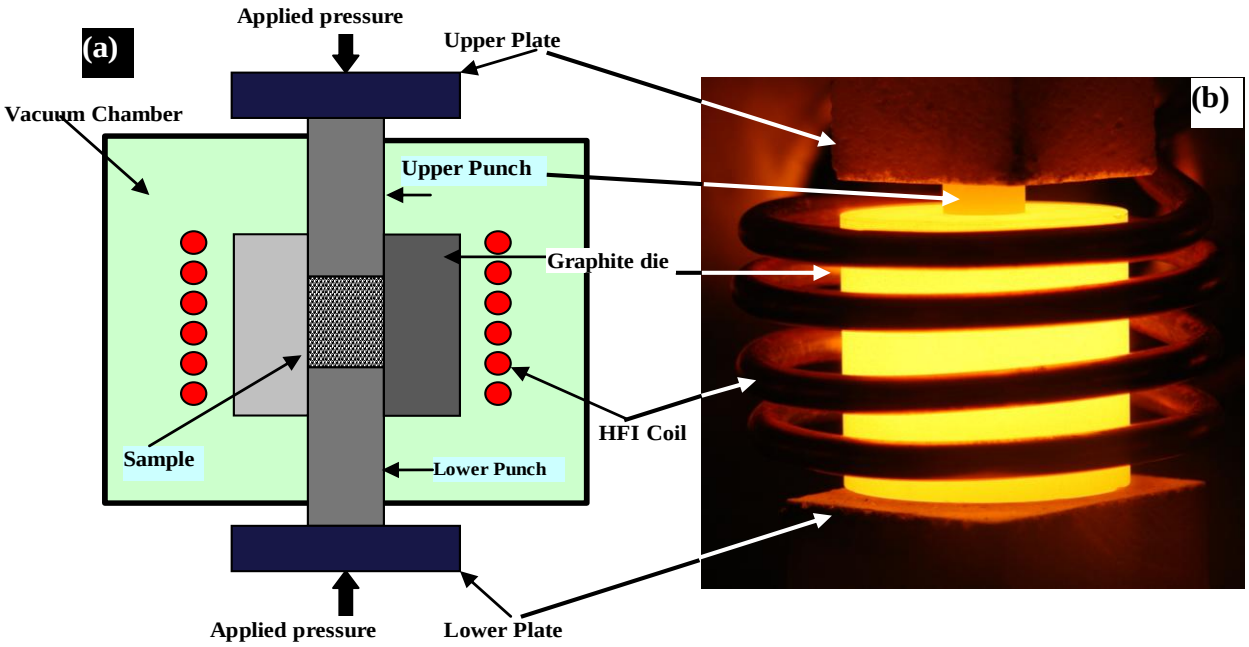

Figure 3. (a) Schematic diagram of high-frequency induction heated sintering apparatus, (b) Photo of the heated die.

It consists of a uniaxial pressure device and a graphite die (outside diameter, 45 mm; inside diameter, 20 mm; height, 40 mm). The unit also features a water-cooled reaction chamber that can be

evacuated, an induced current (frequency of approximately 50 kHz) and pressure-, position- and temperature-regulating systems. HFIHS resembles the hot pressing process in several respects, *i.e.*, the precursor powder is loaded in a die and a uniaxial pressure is applied during the sintering process. However, instead of using an external heating source, an intensive magnetic field is applied through the electrically conducting pressure die and, in some cases, also through the sample. This implies that the die also acts as a heating source and that the sample is heated from both the outside and inside. Temperatures can be measured by a pyrometer focused on the surface of the graphite die. The system is first evacuated to a vacuum level of 1×10^{-3} Torr, and a uniaxial pressure is applied. An induced current (frequency of approximately 50 kHz) is then activated and maintained until densification is observed, indicating the occurrence of sintering and the concomitant shrinkage of the sample. Sample shrinkage is measured by a linear gauge that measures the vertical displacement. The typical parameters for the process are presented in Table 1, and the four major stages of the HFIHS and densification process are shown in Fig. 4.

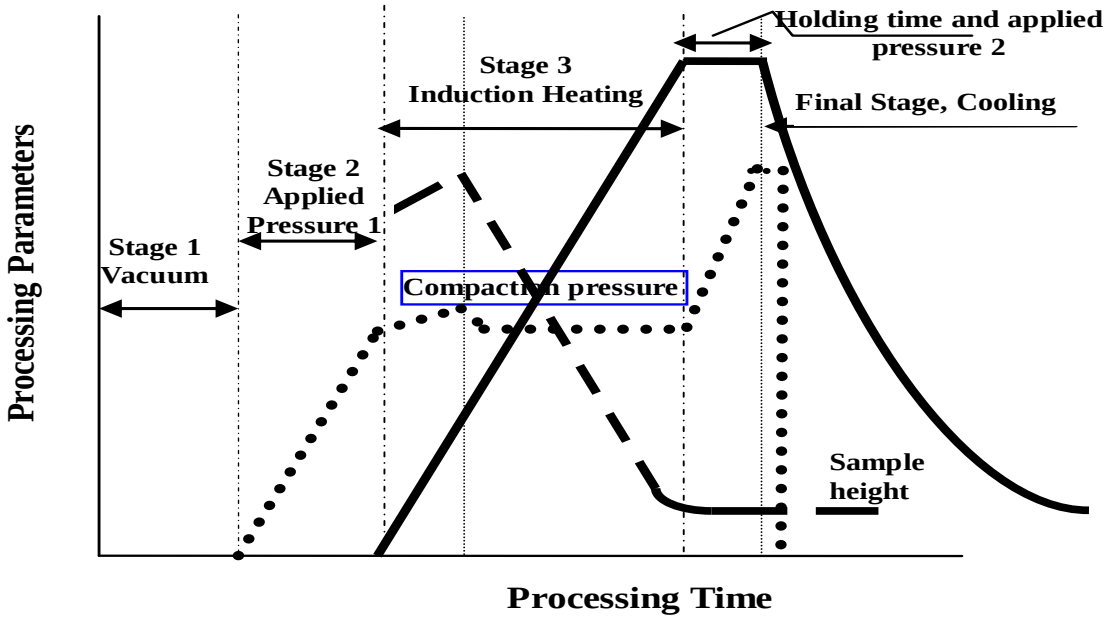

Figure 4. The four major stages of sintering process in the HFIHS apparatus

Table 1. Processing conditions of high-frequency induction heated sintering process

Parameters	Applied value	Parameters	Applied value
Vacuum level	1×10^{-3} Torr	Applied pressure	10 - 300 MPa
Heating rate	100 - 1200 °C/min	Cooling rate	500 °C/min
Total power capacity	15 KW	Output of total power	0 - 100%
Resistance heating Frequency	50 KHz	Duration time	~10 min

After sintering, the samples were ground and polished for subsequent indentation and microscopy studies. The density of the sintered samples was measured by the Archimedes principals. Theoretical density of the Mg-HAp nanocomposites were measured based on the following equation:

$$\rho_{ave} = \frac{100}{\frac{C_1}{\rho_1} + \frac{C_2}{\rho_2}} \quad (1)$$

Where, $\rho_1 = \rho$ (HAp) = 3.16 g/cm^3 and $\rho_2 = \rho$ (Mg) = 1.74 g/cm^3.

The microstructure observations of polished and coated fracture surfaces of the composite were investigated using a Field Emission Scanning Electron Microscope (FE-SEM) (JEOL FESEM 7600 F) coupled with energy dispersive X-ray (EDX) analyzer. The surfaces were coated with platinum to avoid charging during the FE-SEM observation.

Rectangular specimens for the electrochemical test were molded into epoxy resin with only one side of 1 cm^2 exposed to the test solutions. The working surface was grinded successively with metallographic emery paper of increasing fineness up to 1000 grit. The electrode was then cleaned using doubly-distilled water, degreased with acetone, washed using doubly-distilled water again and finally dried with dry air. Electrochemical test was carried out at 37±1 ◦C in a standard three-electrode configuration cell containing 50 mL simulated body fluid (SBF) solution. The SBF solution was prepared by dissolving reagent grade chemicals NaCl, $NaHCO_3$, KCl, $K_2HPO_4.3H_2O$, $MgCl_2.6H_2O$, $CaCl_2$, Na_2SO_4; the solution was buffered at pH 7.4 with 50 mM tris [$(CH_2OH)_3CNH_2$] and 45 mM of hydrochloric acid at 37 ^oC (human body temperature). The ion concentrations in SBF are given in Table 2 along with the ones for human blood plasma [16].

Table 2. Ion concentration (mM) of simulated body fluid (SBF) and human blood plasma (HBP)

	Na^+	K^+	Mg^{2+}	Ca^{2+}	Cl^-	HCO_4^{2-}	HPO_4^{2-}	SO_4^{2-}
SBF	142.0	5.0	1.5	2.5	147.8	4.2	1.0	0.5
HBP	142.0	5.0	1.5	2.5	103.0	27.0	1.0	0.5

A silver/silver chloride was used as a reference and a platinum electrode as the counter and the sample as the working electrode. The electrochemical experiments were performed by using an Autolab Potentiostat (PGSTAT302N computer controlled) operated by the general purpose electrochemical software (GPES) version 4.9. The potentiodynamic polarization curves were obtained by scanning the potential from -2000 to -800 mV against Ag/AgCl at a scan rate of 3.0mV/s. Chronoamperometric current-time (CA) experiments were carried out by stepping the potential of the Mg samples at –1200 mV versus Ag/AgCl after 15 min immersion in SBF. Electrochemical impedance spectroscopy (EIS) tests were performed at corrosion potentials (E_{Corr}) over a frequency range of 100 kHz – 100 mHz, with an ac wave of ± 5 mV peak-to-peak overlaid on a dc bias potential, and the

impedance data were collected using Powersine software at a rate of 10 points per decade change in frequency.

3. RESULTS AND DISCUSSIONS

3.1. Characteristics of the milled powders

Figure 5 shows the EDX analyses of the milled powder. It can be observed that each Mg particle whether it is a small or large is coated with HA particles. EDX analyses clearly showed the presence of Ca, P and O of the HAp in the pure Mg structure. In addition, magnesium rich secondary phase was seen when observed at high magnification. Though the phase structure of HAp was not evident in our XRD analysis, we believe the presence of this phase was responsible for the improvement in physical and mechanical properties of Mg-HAp structures compared to pure Mg.

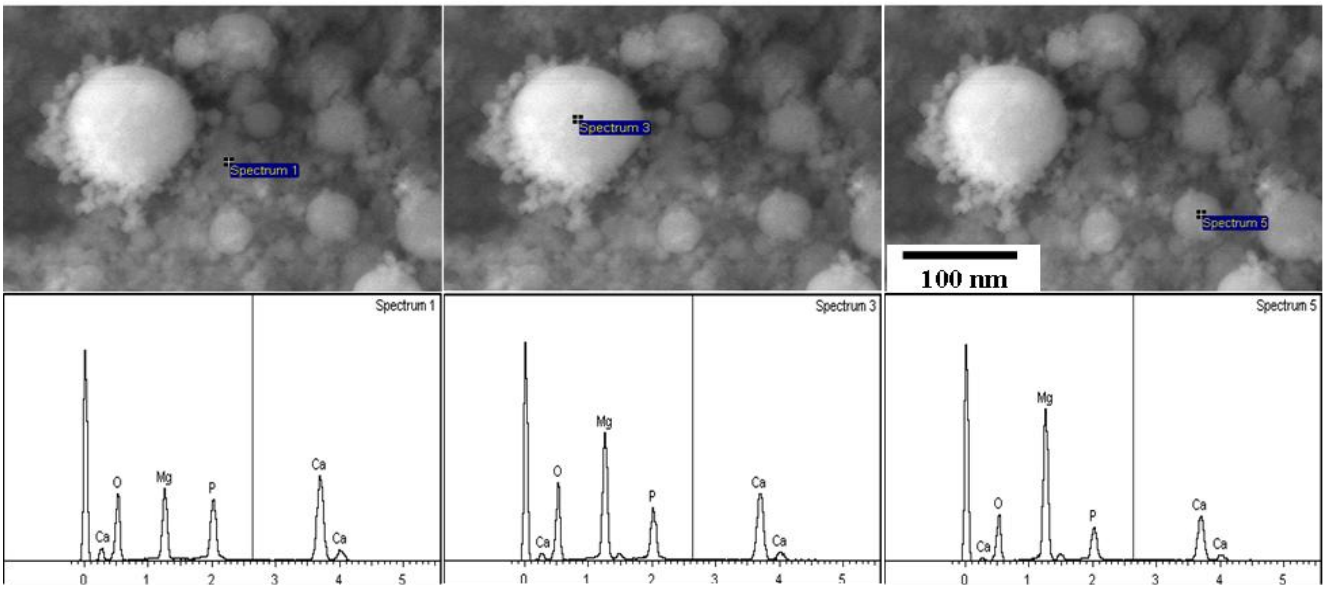

Figure 5. Scanning electron micrograph and EDX plots at three different locations of the Mg/5wt% HAp powder mixture after milling.

3.2. Powder consolidations

Magnesium and its alloys are characterized by the density and Young's modulus close to human bone, non-toxicity and good biocompatibility, thus they are considered a novel promising biodegradable biomaterial. However, due to its high corrosion rate, poor bioactivity and insufficient mechanical strength, magnesium and its alloys are not used in clinics up to now. In this work, an Mg/HAp nanocomposite with various HAp contents (0-5 wt%) have been consolidated very rapidly by HFIHS at constant heating rate around 400 °C/min, constant sintering pressure (60 MPa), temperature (550 °C) and time (3 minutes holding time) in order to develop a new biodegradable hard tissue

substituent possessing the advantages of the both components. Figure 6 shows the density and microhardness of Mg-X wt% HAp compacts. The relative densities of the composites initially increased with increase the amount of HAp addition. We can see that, despite the short dwelling time when the current was applied, the relative density of the sintered samples reached as high as 99.7 % in the composite containing 1% HAp. Microhardness results conducted on Mg and Mg/HAp nanocomposites are shown in Fig 6. The results of hardness measurements revealed an increase in microhardness values with increasing weight percentage of nano-size HAp reinforcement into the magnesium matrix to a certain level and then decreased. Among the nanocomposite formulations, magnesium reinforced with 1 to 3 wt% of HAp nanopowder showed the best overall improvement in both relative density and hardness. The hardness of Mg reinforced with 1 to 3 wt% HAp 70 HV as well as the relative density reached as high as 99.7%. The reason for the increase in Relative density and microhardness is probably due to the presence of HAp fragmented nanoparticles at the grain boundary regions. These nanosized inclusions can significantly enhance the mechanical properties of Mg. Remarkably, with increasing HAp content more than 3 wt% HAp, the relative density and microhardness decreased. Decreasing in relative density and microhardness of the nano composites with increasing HAp content can be attributed to two reasons. First, some degree of HAp nanoparticle clustering takes place. Second, the sintering temperature of pure HAp is almost around 1000 °C, with increasing HAp content in the Mg matrix, 550 °C the sintering temperature become not enough for densifications. Notably, increasing sintering temperature is not possible due to low melting temperature of Mg matrix. The hardness values for all of the Mg/HAp nanocomposite samples have narrow distribution ranges, indicating a homogeneous distribution of the HAp phase in the Mg matrix.

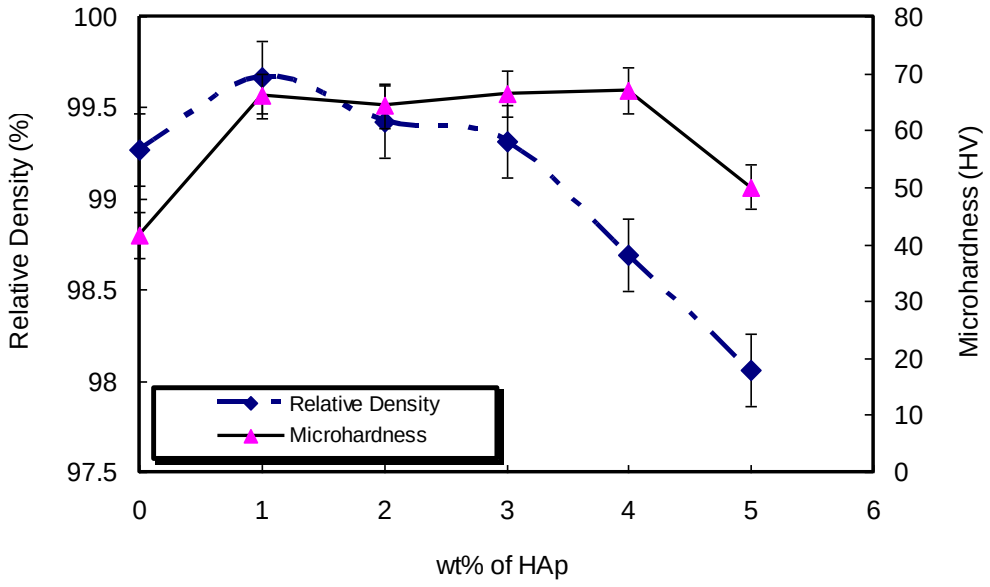

Figure 6. Effects of hydroxyapatite additions on the relative density and microhardness of Mg/Hap nanocomposites

3.3. Potentiodynamic polarization measurements

Figure 7 shows the potentiodynamic polarization curves for (a) Mg/0.0wt% HAp, (b) Mg/1.0wt% HAp, (c) Mg/2.0wt% HAp, (d) Mg/3.0wt% HAp, (e) Mg/4.0wt% HAp, and (f) Mg/5.0wt% HAp, respectively after 15 min immersion in the SBF solutions.

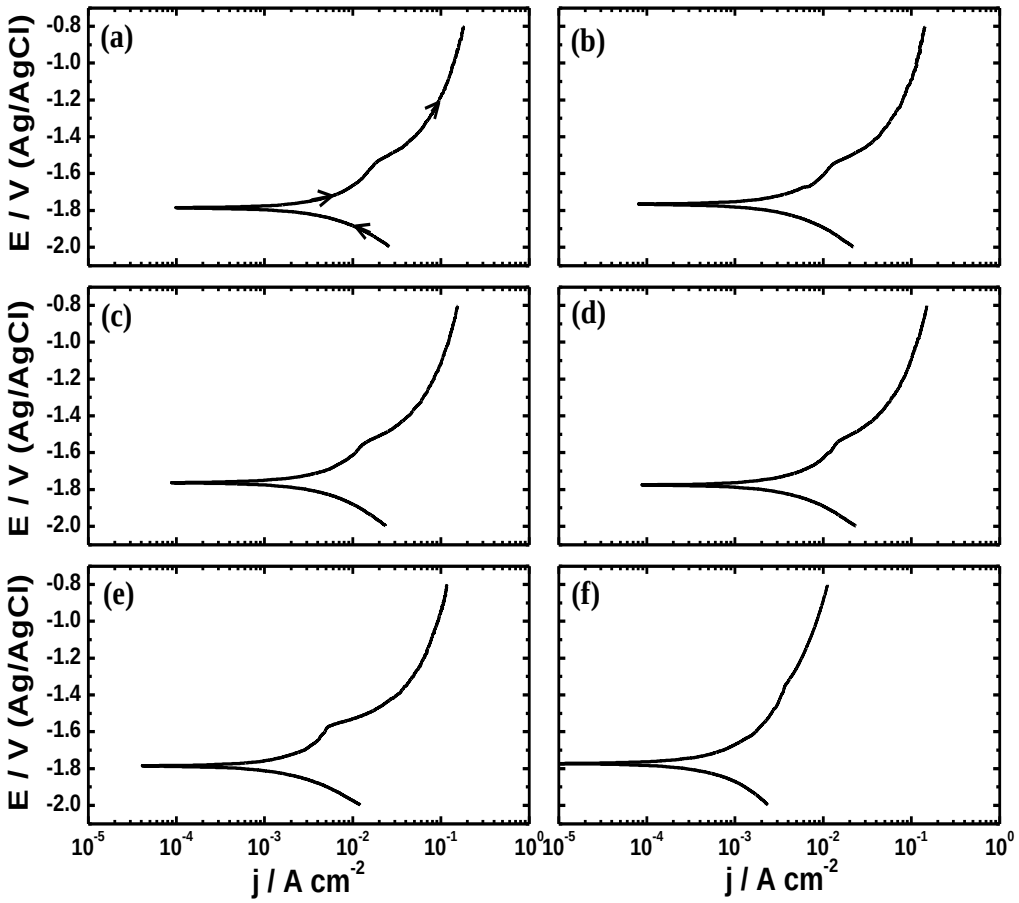

Figure 7. Potentiodynamic polarization behavior of (a) Mg/0.0wt% HAp, (b) Mg/1.0wt% HAp, (c) Mg/2.0wt% HAp, (d) Mg/3.0wt% HAp, (e) Mg/4.0wt% HAp, and (f) Mg/5.0wt% HAp after 15 min immersion in simulated body fluid

The polarization experiments were carried out in order to obtain the corrosion parameters like corrosion potential (E_{Corr}), corrosion current (j_{Corr}), polarization resistance (R_P), and corrosion rate (K_{Corr}) of Mg with and without HAp in the test solutions. Here, the cathodic reaction for Mg in the SBF is the hydrogen evolution as the electron consumption on magnesium happens by the unloading of hydrogen ions (acidic corrosion), as follows [17],

$$2H^+ + 2e^- = H_2 \qquad (2)$$

The source of the hydrogen ions (more exactly the hydronium ion H_3O) is the dissociated water, as shown below;

$$H_2O = H^+ + OH^- \quad (3)$$

The anodic reaction that causes the dissolution of Mg occurs once the metal is in contact with the test electrolyte according to [18, 19];

$$2Mg = 2Mg^{2+} + 4e^- \quad (4)$$

The anodic reaction also includes the formation of magnesium oxide as follows;

$$Mg + O = MgO \quad (5)$$

Because of secondary reactions, magnesium cations (reactions 3) will react with the hydroxide ions produced in reaction (2) as follows;

$$Mg^{2+} + 2OH^- = Mg(OH)_2 \quad (6)$$

Table 3. Corrosion parameters obtained from polarization curves shown in Fig. 7 for the different magnesium alloys in the SBF solutions.

Sample	Parameter						
	β_c / mV dec^{-1}	E_{Corr}/ mV	j_{Corr} / μA cm^{-2}	β_a / mV dec^{-1}	E_{Pit} / mV	R_p / Ω cm^2	K_{Corr}/ mmy^{-1}
Mg/0.0wt% HAp	185	-1775	2900	160	-1535	12.86	66.26
Mg/1.0wt% HAp	175	-1770	2400	170	-1545	15.62	54.83
Mg/2.0wt% HAp	170	-1775	2200	180	-1555	17.28	50.26
Mg/3.0wt% HAp	155	-1778	2050	185	-1555	17.89	46.84
Mg/4.0wt% HAp	140	-1785	1050	200	-1580	34.10	23.99
Mg/5.0wt% HAp	140	-1794	350	210	–	104.35	8.00

Table 3 presents the calculated values of the values of the cathodic (β_c) and anodic (β_a) Tafel slopes, corrosion potential (E_{Corr}), corrosion current (j_{Corr}), pitting potentials (E_{Pit}), polarization resistance (R_P), and corrosion rate (K_{Corr}) from polarization curves shown in Fig. 7. It is clearly seen from Fig. 7a that an active dissolution of the alloy occurred with increasing potential in the anodic side under the aggressiveness action of the SBF solution. It is also seen that the presence of HAp and the increase of its content with Mg, Fig. 7b-f, decreased the dissolution of Mg. This was confirmed by the decrease of the values of cathodic, j_{Corr}, and anodic currents and K_{Corr}, as well as the negative shift in the values of E_{Corr} and the increase of R_P. On the other hand, this effect increased the pitting corrosion as the E_{Pit} increased to the more negative values. It is worth mentioning that the values of E_{Corr} and j_{Corr}

were obtained from the extrapolation of anodic and cathodic Tafel lines located next to the linearized current regions. The values of R_P and K_{Corr} were calculated from the polarization data as reported in our previous work [19–27]. This indicates that the presence of HAp and the increase of its content improve the resistance of magnesium against uniform corrosion, while increase the probability of the occurrence of localized corrosion. The localized corrosion here might occur due to the HAp particles have higher noble potential than that for magnesium.

3.4. Chronoamperometric current-time measurements

In order to shed more light on the effects of HAp on improving the corrosion resistance of magnesium in SBF solution at more positive potential than the corrosion potential, E_{Corr}, chronoamperometric potentiostatic current–time experiments were carried out. The chronoamperometric current-time curves for (1) Mg/0.0wt% HAp, (2) Mg/1.0wt% HAp, (3) Mg/2.0wt% HAp, (4) Mg/3.0wt% HAp, (5) Mg/4.0wt% HAp, and (6) Mg/5.0wt% HAp were collected at -1200 mV vs. Ag/AgCl after 15 min immersion in SBF solution are shown in Fig. 8. The value of the constant potential was determined from polarization curves. It is obvious from Fig. 7 that the highest current was recorded for pure magnesium, Fig. 7 (curve 1). At this condition, the current showed a rapid increase in its initial values due to the dissolution of an oxide film might have formed on the surface of Mg during its immersion in the test solution. The current then slightly increased and decreased accompanied by small fluctuations with a slow and slight absolute current decrease at the end of the run. This current behavior indicates that the Mg electrode suffers pitting corrosion.

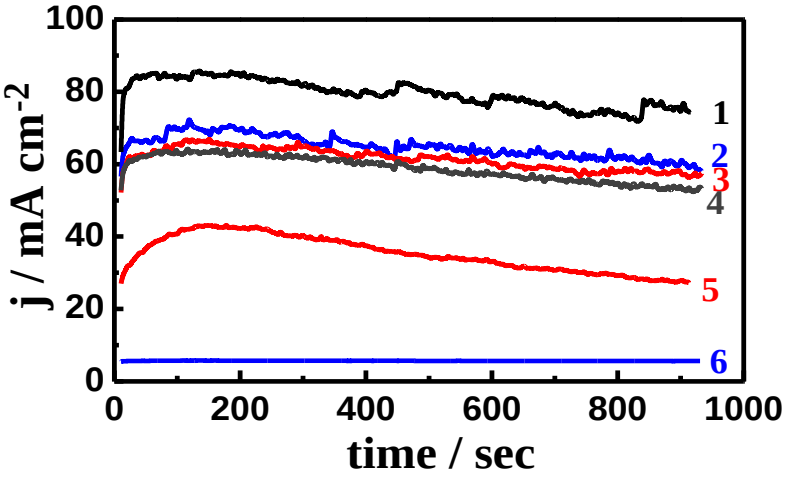

Figure 8. Chronoamperometric curves collected at -1200 mV vs. Ag/AgCl for (1) Mg/0.0wt% HAp, (2) Mg/1.0wt% HAp, (3) Mg/2.0wt% HAp, (4) Mg/3.0wt% HAp, (5) Mg/4.0wt% HAp, and (6) Mg/5.0wt% HAp after 15 min immersion in simulated body fluid

The presence of 1.0wt% HAp, Fig. 8 (curve 2), shows almost the same behavior but with lower absolute current values, which indicates that the presence of 1.0wt% HAp decreases the uniform

corrosion. Similar behavior but with lower absolute current values was also recorded when the concentration of HAp was increased to 4.0wt% as shown in Fig. 8, curve 3 and curve 4. The best performance against corrosion in SBF solution was obtained for Mg/5.0wt%HAp, Fig. 8 curve 5. This confirms the data obtained by polarization indicating that the presence of HAp and the increase of its content increase the corrosion resistance of magnesium in SBF solution.

3.5. Electrochemical impedance spectroscopy (EIS) investigation

The EIS experiments here were carried out to determine kinetic parameters for electron transfer reactions at the electrode/electrolyte interface. The method was successfully employed to explain the corrosion and passivation phenomena of metals and alloys [19-34]. Typical Nyquist plots taken at open circuit potential for (a) Mg/0.0wt% HAp, (b) Mg/1.0wt% HAp, (c) Mg/2.0wt% HAp, (d) Mg/3.0wt% HAp, (e) Mg/4.0wt% HAp, and (f) Mg/5.0wt% HAp after 15 min immersion in the SBF solution are shown in Fig. 9.

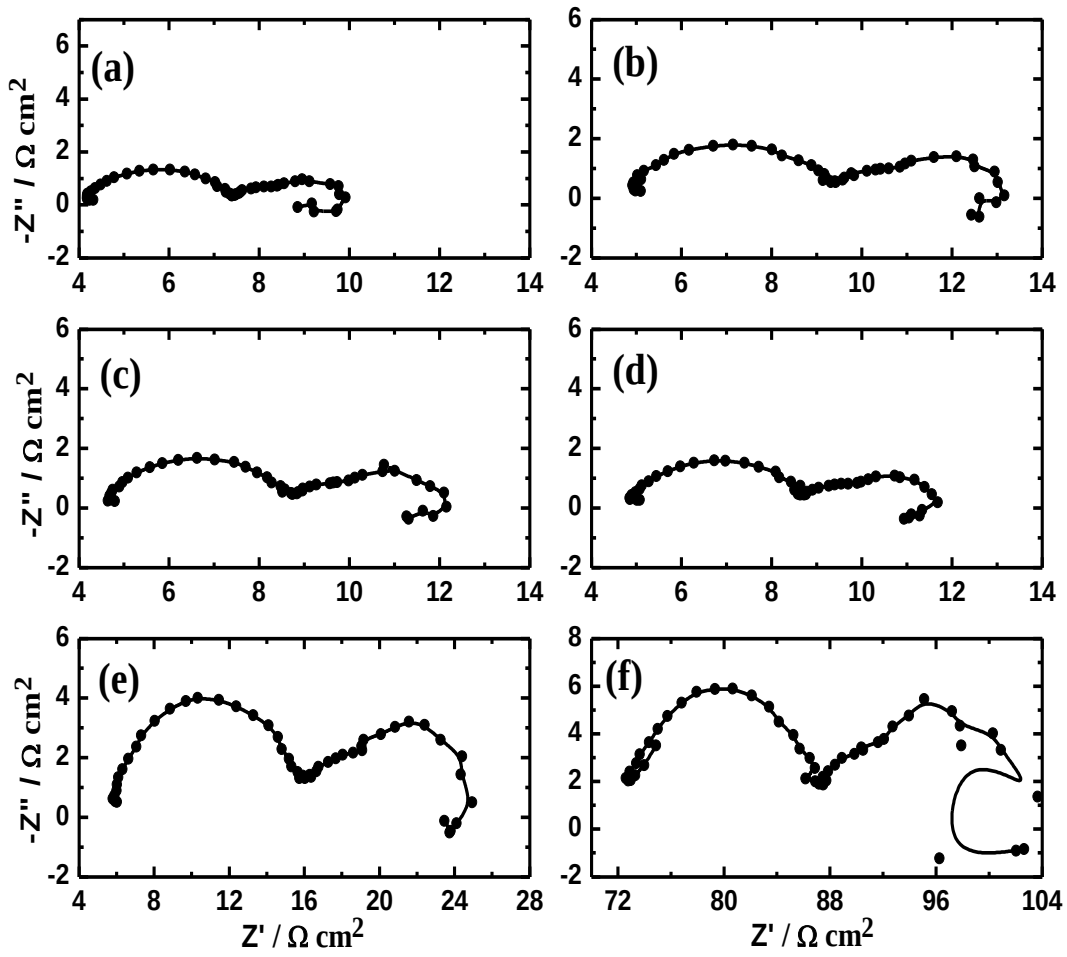

Figure 9. Typical Nyquist plots for (a) Mg/0.0wt% HAp, (b) Mg/1.0wt% HAp, (c) Mg/2.0wt% HAp, (d) Mg/3.0wt% HAp, (e) Mg/4.0wt% HAp, and (f) Mg/5.0wt% HAp after 15 min immersion in simulated body fluid.

The impedance spectrum for the Nyquist plots were analysed by fitting to the equivalent circuit model for the case with two time constants as shown in Fig. 10. The values of the parameters obtained by fitting the equivalent circuit are listed in Table 2. These parameters are defined as follows; R_S represents the solution resistance, C_{dl1} a double layer capacitance, R_{P1} the polarization resistance and can be referred also as the charge transfer resistance (R_{ct}), Q the constant phase elements (CPEs), R_{P2} another polarization resistance. This circuit also includes another double layer capacitance, (C_{dl2}) which is placed in parallel to charge transfer resistance element R_{P3}. The Nyquist plots of Fig. 9 thus manifested two depressed capacitive semicircles at higher and lower frequencies regions. The experimental data were consistent with the involvement of the intermediate species Mg^+ in magnesium dissolution at film imperfections or on a film-free surface. At such sites, magnesium is first oxidised electrochemically to intermediate species Mg^+, then the intermediate species react chemically with water to produce hydrogen and Mg^{2+} [35]. The low frequency locus displays the characteristics of a parallel RC circuit. The R_{P3} value is a measure of charge transfer resistance corresponding to the reaction [35].

$$Mg^+ = Mg^{2+} + e^- \qquad (7)$$

Table 4. Impedance parameters obtained by fitting the Nyquist plots shown in Fig. 9 with the equivalent circuit shown in Fig. 10 for the magnesium alloys in SBF solutions.

Parameter Alloy	R_S / Ω cm^2	C_{dl1} / μFcm^{-2}	R_{p1} / Ω cm^2	Q		R_{p2} / Ω cm^2	C_{dl2} / μFcm^{-2}	R_{p3} / Ω cm^2
				Y_Q / μF cm^{-2}	n			
Mg/0.0wt% HAp	4.18	0.592	5.162	91.54	0.81	7.472	0.237	5.3
Mg/1.0wt% HAp	4.94	0.533	7.464	90.25	0.78	7.917	0.1971	6.01
Mg/2.0wt% HAp	4.66	0.514	8.823	87.36	0.78	9.491	0.2187	7.41
Mg/3.0wt% HAp	4.89	0.408	9.274	70.16	0.80	11.827	0.1971	8.25
Mg/4.0wt% HAp	5.85	0.388	12.68	20.99	0.80	13.346	0.1417	11.87
Mg/5.0wt% HAp	7.65	0.211	16.82	0.296	0.80	42.677	0.1326	15.96

It is clearly seen from Fig. 9 and Table 4 that the values of resistances, R_S, R_{P1}, R_{P2} and R_{P3} increase in the presence of HAp and the increase of its content from 1wt% to 5 wt%. The increase in resistivity arises from the change in chemical composition of the surface film due to the incorporation of HAp into the film especially through defect sites with low ionic resistance. This effect also decreased the values of the C_{dl1}, *CPE,* and C_{dl2} and indicates that HAp particles improve the corrosion resistance of magnesium in SBF solution and its effect increases with increasing HAp concentration. This was also confirmed by the Bode impedance plots shown in Fig. 8 for (1) Mg/0.0wt% HAp, (2) Mg/1.0wt% HAp, (3) Mg/2.0wt% HAp, (4) Mg/3.0wt% HAp, (5) Mg/4.0wt% HAp, and (6) Mg/5.0wt% HAp after 15 min immersion in SBF solution, where the impedance of the interface (|Z|) of Mg increased in the presence and by the increase of HAp. According to our previous studies [28-30, 37-39], the increase in the values of |Z|, especially at low frequency region, means the better the

corrosion resistance of the surface. The EIS measurements are thus in good agreement with the data obtained by polarization and chronoamperometry.

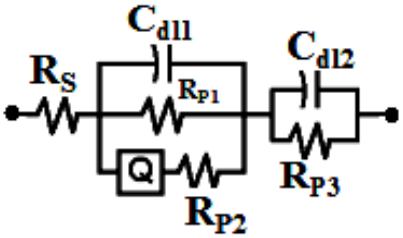

Figure 10. The equivalent circuit used to fit the experimental data presented in Fig. 9.

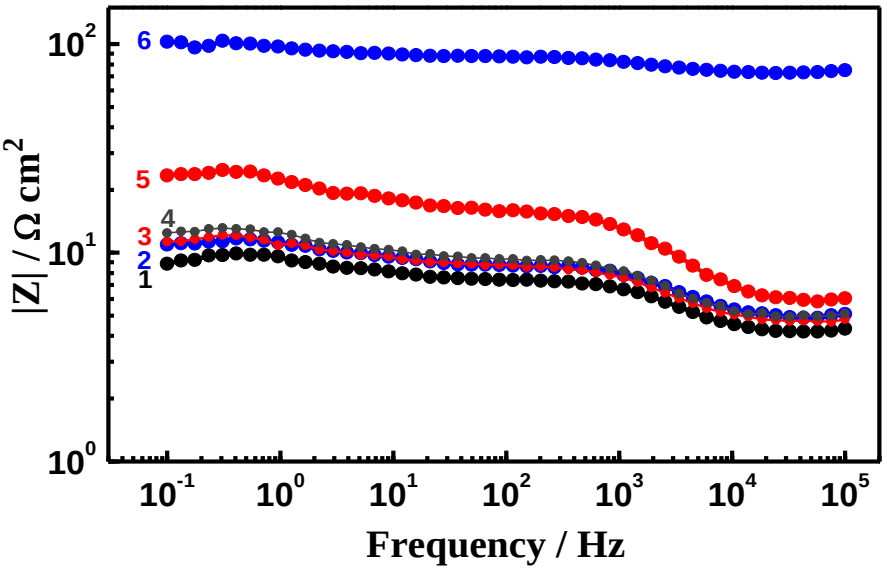

Figure 11. Bode impedance plots for (1) Mg/0.0wt% HAp, (2) Mg/1.0wt% HAp, (3) Mg/2.0wt% HAp, (4) Mg/3.0wt% HAp, (5) Mg/4.0wt% HAp, and (6) Mg/5.0wt% HAp after 15 min immersion in simulated body fluid.

4. CONCLUSIONS

Mg/HAp nanocomposite with various HAp contents (0-5 wt %) were successfully super fast densified in a very short time using high frequency induction heat sintering. The attendant corrosion features of this nanocomposite were investigated and the conclusion can be excluded as follows:

1. The polarization experiments were carried out in order to obtain the corrosion parameters like corrosion potential (E_{Corr}), corrosion current (j_{Corr}), polarization resistance (R_P), and corrosion rate (K_{Corr}) of Mg with and without HAp in the test solutions.

2. An active dissolution of the alloy occurred with increasing potential in the anodic side under the aggressiveness action of the SBF solution. The presence of HAp and the increase of its

content, decreased the dissolution of Mg and improve the resistance of magnesium against uniform corrosion, while increase the probability of the occurrence of localized corrosion.

3. The best performance against corrosion in SBF solution was obtained for Mg/5.0wt%HAp. This confirms the data obtained by polarization.

4. The EIS experiments were carried out to determine kinetic parameters for electron transfer reactions at the electrode/electrolyte interface magnesium in SBF solution. The values of resistances, R_S, R_{P1}, R_{P2} and R_{P3} increased in the presence of HAp and the increase of its content from 1wt% to 5 wt%. This effect also decreased the values of the C_{dl1}, *CPE*, and C_{dl2} and indicates that HAp particles improve the corrosion resistance of magnesium in SBF solution and its effect increases with increasing HAp concentration.

5. The impedance of the interface (|Z|) of Mg increased in the presence and by the increase of HAp content. The EIS measurements are thus in good agreement with the data obtained by polarization and chronoamperometry.

6. In this work, the Mg/1 to 3 wt% HAp composite was of the optimal mechanical properties and corrosion resistance.

ACKNOWLEDGEMENTS

This work was financially supported by the Center of Excellence for Research in Engineering Materials (CEREM), College of Engineering, King Saud University, project No. 430-CEREM-04.

References

1. F. Witte, V. Kaese, H. Haferkamp, E. Switzer, A. Meyer-Lindenberg, C.J. Wirth, *Biomaterials*, 26 (2005) 3557.
2. F. Witte, J. Fischer, J. Nellesen, H.-A. Crostack, V. Kaese, A. Pisch, et al., *Biomaterials*, 27 (2006) 1013.
3. L. Xu, G. Yu, E. Zhang, F. Pan, K. Yang, *J. Biomed. Mater. Res*. 83 (2007) 703.
4. M.P. Staiger, A.M. Pietak, J. Huadmai, G. Dias, *Biomaterials*, 27 (2006) 1728.
5. G. Song, Corros. Sci., 49 (2007) 1696.
6. D. Yin, E. Zhang, S. Zeng, *Trans. Nonferrous Metal. Soc*.18 (2008) 763.
7. E. Zhang, D. Yin, L. Xu, L. Yang, K. Yang, *Mater. Sci. Eng. C, in press*, doi:10.1016/j.msec.2008.08.024.
8. L. Xu, E. Zhang, D. Yin, S. Zeng, K. Yang, *J. Mater. Sci*., 19 (2008) 1017.
9. M. Jarcho, C.H. Bolen, M.B. Thomas, J. Bobick, J.F. Kay, R.H. Doremus, *J. Mater. Sci*., 11 (1976) 2027.
10. K.A. Khalil, S.W. Kim , K.W. Kim, N. Dharmaraj, H.Y. Kim, *Int. J. Appl. Ceram. Techol*., 8 (2011) 523.
11. S.W. Kim, S.L. Cockcroft, K.A. Khalil, K. Ogi, *Mater. Sci. Eng*. A, 527 (2010) 4926.
12. K.A. Khalil, S.W. Kim, H.Y. Kim, *Mater. Sci. Eng*. A, 456 (2007) 368.
13. K.A. Khalil, S.W. Kim, H.Y. Kim, *Int. J. Appl. Ceram. Techol*., 4 (2007) 30.
14. K.A. Khalil, S.W. Kim, N. Dharmaraj, K.W. Kim, H.Y. Kim, *J. Mater. Process. Techol*., 187-188 (2007) 417.
15. K.A. Khalil, S.W. Kim, *Trans. Nonferrous Met. Soc. China*, 17(2007) 21.
16. Y. Ebisawa, F. Miyaji, T. Kokubo, K. Ohura, T. Nakmura, *J. Biomat.* 18 (1997) 1277.
17. S. Bender, J. Goellner, A. Heyn, E. Boese, *Mater. Corros*., 58 (2007) 977.

18. Zhiming Shi, Andrej Atrens, *Corros. Sci*., 53 (2011) 226.
19. El-Sayed M. Sherif, Abdulhakim A. Almajid, *Int. J. Electrochem. Sci*., 6 (2011) 2131.
20. El-Sayed M. Sherif, J. H. Potgieter, J. D. Comins, L. Cornish, P. A. Olubambi, C. N. Machio, *J. Appl. Electrochem*., 39 (2009) 1385.
21. El-Sayed M. Sherif, J. H. Potgieter, J. D. Comins, L. Cornish, P. A. Olubambi, C. N. Machio, *Corros. Sci*., 51 (2009) 1364.
22. El-Sayed M. Sherif, A. A. Almajid, F. H. Latif, H. Junaedi, *Int. J. Electrochem. Sci.*, 6 (2011) 1085.
23. El-Sayed M. Sherif, A. A Almajid, *J. Appl. Electrochem*., 40 (2010) 1555.
24. El-Sayed M. Sherif, *Int. J. Electrochem. Sci*. 6 (2011) 1479.
25. El-Sayed M. Sherif, A. H. Ahmed, *Synthesis and Reactivity in Inorganic, Metal-Organic, and Nano-Metal Chemistry*, 40 (2010) 365.
26. El-Sayed M. Sherif, R. M. Erasmus, J. D. Comins, *Electrochim. Acta*, 55 (2010) 3657.
27. El-Sayed M. Sherif, *J. Mater. Eng. Perform.*, 19 (2010) 873.
28. El-Sayed M. Sherif, R.M. Erasmus, J.D. Comins, *J. Colloid Interface Sci*., 311 (2007) 144.
29. El-Sayed M. Sherif, R.M. Erasmus, J.D. Comins, *J. Colloid Interface Sci*., 306 (2007) 96.
30. El-Sayed M. Sherif, R.M. Erasmus, J.D. Comins, *J. Colloid Interface Sci*., 309 (2007) 470.
31. El-Sayed M. Sherif, R.M. Erasmus, J.D. Comins, *Corros. Sci*., 50 (2008) 3439.
32. El-Sayed M. Sherif, *Int. J. Electrochem. Sci*., 6 (2011) 2284.
33. El-Sayed M. Sherif, *Int. J. Electrochem. Sci*., 6 (2011) 3077.
34. El-Sayed M. Sherif, *Mater. Chem. Phys*., 129 (2011) 961.
35. A.M. Fekry, M.A. Ameer, *Int. J. Electrochem. Sci*., 6 (2011) 1342.
36. E.M. Sherif, S.-M. Park, *J. Electrochem. Soc*., B 152 (2005) 205.
37. E.M. Sherif, S.-M. Park, *Electrochim. Acta*, 51 (2006) 1313.
38. E.M. Sherif, S.-M. Park, *Electrochim. Acta*, 51 (2006) 4665.
39. El-Sayed M. Sherif, *J. Appl. Surf. Sci*., 252 (2006) 8615.